ELSEVIER

Contents lists available at ScienceDirect

Organic Electronics

journal homepage: www.elsevier.com/locate/orgel





Perovskite films passivated by poly[(R)-3-hydroxybutyric acid] for improved photovoltaic performance

Yifang Qi^a, Jing Qu^a, Jaiden Moore^a, Kristine Gollinger^a, Narendra Shrestha^b, Yongfeng Zhao^a, Nihar Pradhan^a, Jinke Tang^b, Qilin Dai^{a,*}

ARTICLE INFO

Keywords:
Poly[(R)-3-Hydroxybutyric acid])
Passivation
C=O
Polymer
Perovskite solar cells

ABSTRACT

Polymer is one of the most effective passivation additives in perovskite solar cells (PSCs). Herein, we apply a polymer Poly[(R)-3-hydroxybutyric acid]) (PHB) to passivate the defects and traps in the perovskite films due to the presences of C=O functional group in the structure of PHB. The FTIR result demonstrates the PHB has chemical interaction with perovskite films, which can decrease the Pb trap density on the surface of films. As a result, the PCE of PSCs increases from 18.92% to 20.20%, and the average Voc increases from 1.07 V to 1.11 V due to PHB passivation. The hydrophobic properties of the alkyl chains on the polymer enhance the stability of the devices. The device without PHB passivation degrades to $\sim\!\!72\%$ of the initial PCE, whereas the PCE of the device with PHB still exhibit 98% of its initial PCE as the devices are kept under 25 \pm 5% RH and 30 \pm 5 °C condition for 14 days. For high humidity condition (60 \pm 5% RH for 350 min), The device with PHB can keep \sim 75% of the original PCE value, but the control device can only maintain $\sim\!\!45\%$ of the initial value. This work presents a new strategy to increase the efficiency and stability of PSCs by two function groups C=O and alkyl chains

1. Introduction

In the past few years, perovskite solar cells (PSCs) have attracted great interests due to the unique properties of perovskite films, including simple processing methods [1,2], the high absorption coefficient [3,4], long carrier lifetime [5,6], and low exciton binding energy [7,8]. Thus, the PSCs are considered as the next-generation photovoltaic devices, which the power conversion efficiency (PCE) has reached 25.7% [9]. However, the nonradiative recombination and defects are still present at the surface and grain boundaries of perovskite films, leading to PCE loss and poor stability of the PSCs [10–12].

The perovskite film quality can influence the charge extraction, charge transport, hysteresis behavior of the devices. Therefore, the quality of perovskite film plays a key role in obtaining high PCE. Various techniques were developed to obtain defect-free and excellent surface coverage films such as vacuum thermal evaporation method [13,14], vapor transport deposition method [15], and passivation additive method [16], and the most effective method is the passivation of perovskite films by the suitable passivation additives. Many organic

molecules were used to passivate perovskite films to improve the film quality and enhance the performance of devices [17,18]. Several functional groups in the organic molecular materials structure are demonstrated to improve the performance of devices [17,19]. Tae-Hee Han et al. demonstrated carbonate groups in poly(propylene carbonate) can effectively decrease the defect density in the perovskite films. Carbonate functional groups as a Lewis base donate the lone pair electrons to the perovskite precursors [20]. Min Zhong et al. studied the influence of polyethylene glycol (PEG) and polyvinylpyrrolidone (PVP) with carbon-oxygen double bond groups on the performance of PSCs, which indicated the carbon-oxygen double bond functional groups could interact with Pb²⁺ in the perovskite films and further eliminate the traps [21]. Afroz et al. studied the influence of -COOH functional groups on the PCE of PSCs. The average PCE of devices increased from 14.06% to 17.12% after -COOH functional group treatment [19]. It is highly demanded that one polymer applied to passivate the PSCs can not only improve the morphology of perovskite films to enhance the PCE, but also protect the PSCs from degradation by moisture due to the hydrophobic properties of polymer [22,23]. It is reported that the C=O functional

E-mail address: qilin.dai@jsums.edu (Q. Dai).

a Department of Chemistry, Physics, and Atmospheric Sciences, Jackson State University, Jackson, MS, 39217, United States

^b Department of Physics & Astronomy, University of Wyoming, Laramie, WY, 82071, USA

 $^{^{\}star}$ Corresponding author.

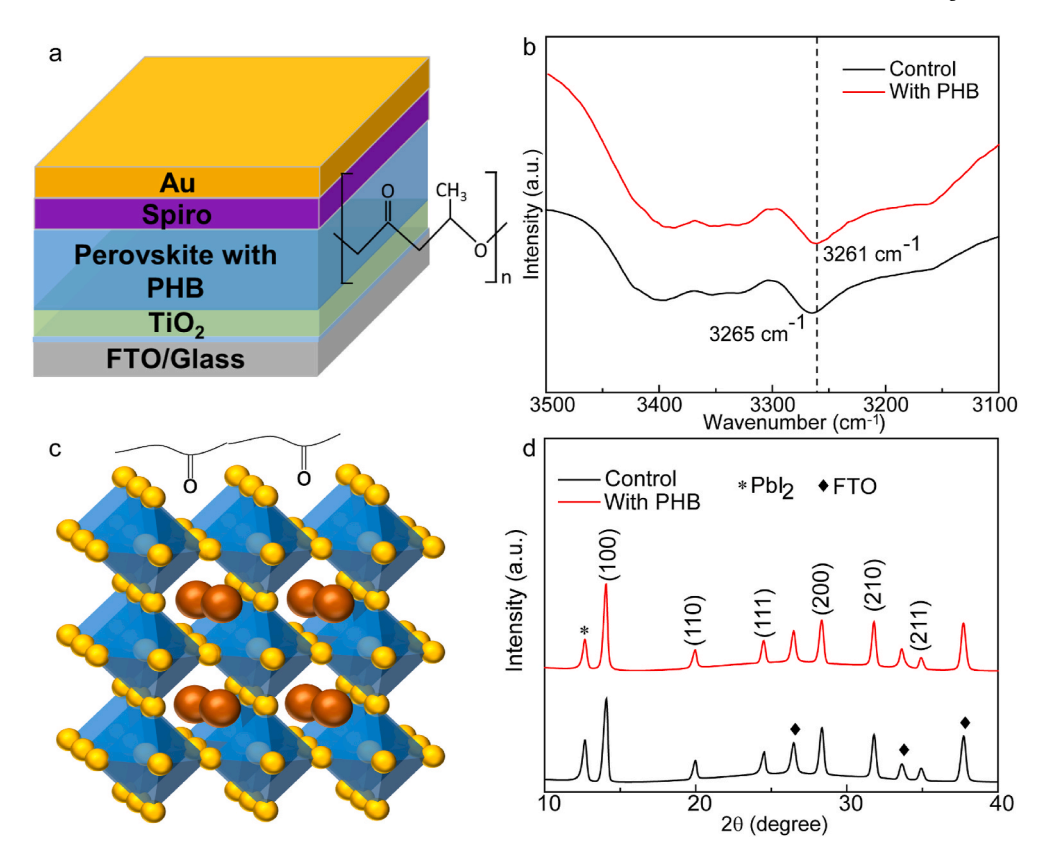


Fig. 1. a The structure of the PSCs. The inset shows the PHB molecular structure; b The FTIR spectra of perovskite films with and without PHB; c The passivation principle of perovskite modified with PHB; d The XRD diffraction patterns of the perovskite films with and without PHB.

groups can denote the lone pair electrons to the perovskite films and further enhance the performance of the PSCs [9,24–27]. PHB is a polymer with C=O functional groups on the mail chain, and the alkane groups in PHB exhibit potential to improve the device stability. Therefore, PHB is very promising for PSC passivation.

Herein, we study the influence of PHB on the PSCs performance, which is introduced by the post-treatment method. The PHB can interact with perovskite films due to the C=O functional groups in the PHB structure. The champion device with PHB passivation exhibits the PCE of 20.20% with Jsc of 24.36 mA/cm², Voc of 1.11 V and FF of 74.26%, which is higher than the control device with PCE of 18.92%, Jsc of 23.90 mA/cm², Voc of 1.07 V and FF of 73.67%. Furthermore, the hysteresis behavior of the PSCs is suppressed by the PHB passivation. The hysteresis index values of the PSCs with and without PHB passivation are 0.002 and 0.061, which indicates that the PHB passivation reduces the nonradiative recombination in the perovskite films. In addition, the PHB passivation improves the device stability due to the hydrophobic properties of alkyl chains. Under humidity conditions (60 \pm 5% RH for 350 min), the PSCs with the PHB passivation can keep \sim 75% of the original values of PCE, but the control devices only can maintain ~45% of the initial values.

2. Materials and experiments

2.1. Materials

Lead iodide (PbI₂, 99%), titanium (IV) chloride (TiCl₄, 99.9%), dimethyl sulfoxide (DMSO, 99.8% anhydrous) and gold (Au, wires) were purchased from Alfa Aesar (America). Lead (II) bromide (PbBr₂, 99%) was obtained from Chemsavers. Poly[(R)-3-hydroxybutyric acid], formamidine iodide (FAI, 99%), cesium iodide (CsI, 98%), methylammonium bromide (MABr, 99.9%), chlorobenzene (CB, 99.8% anhydrous), and 2,2′,7,7′-Tetrakis[N,N-di(4-methoxyphenyl)amino]-

9,9'-spirobifluorene (Spiro-OMeTAD) were purchased from Sigma Aldrich (America). Lithium bi(trifluoromethane) sulfonimide (Li-TFSI) were obtained from TCI (Japan). 4-tert-butylpyridine(4-tBP) was purchased from Accela (America). Patterned fluorine doped tin oxide glass substrates were received from Advanced Election Technology Co., Ltd (China). All chemical materials were applied without further purification treatment.

2.2. Device fabrication

The etched FTO glass substrates were cleaned by detergent solution, acetone, deionized water, and isopropanol in the ultrasound water bath for 15 min, sequentially. Then the substrates were dried by air flowing, then the substrates were treated with ultraviolet-ozone treatment for 30 min. The cleaned FTO glass substrates were immersed in 0.2 M TiCl₄ aqueous solution (prepared at 0 °C) and kept at 60 °C by a water bath for 60 min to fabricate TiO₂ electron transport layers. Then, the redundant TiO₂ particles on the substrates were washed away by deionized water and isopropanol followed by annealing at 200 °C for 30 min to form the FTO/TiO2 films. Afterwards, the films were transferred to the N2 glovebox to fabricate the others layers in the devices. The perovskite precursor solution was prepared by 1.1 M PbI2, 0.2 M PbBr2. 0.2 M MABr and 1 M FAI in the mixed solvents (DMF: DMSO = 4:1, volume ratio). Then 40 µL CsI solution (1.5 M in 1 mL DMSO) was added into the perovskite precursor solution. The perovskite wet films were prepared by the anti-solvent method, in which the perovskite precursor solution was spin-coated on TiO2 layer with 4000 rpm for 40 s, and then chlorobenzene as anti-solvent was dropped on the spinning substrates with 4000 rpm at the last 20 s. Next, the wet films were annealed at 100 $^{\circ}$ C for 60 min to form $Cs_{0.05}(FA_{0.83}MA_{0.17})_{0.95}Pb(I_{0.83}Br_{0.17})_3$ perovskite films. After that, PHB as a passivation layer with different concentrations dispersed in isopropanol solvent was spin-coated onto the perovskite films and the films were annealed at 70 $^{\circ}\text{C}$ for 10 min. PHB molecules are

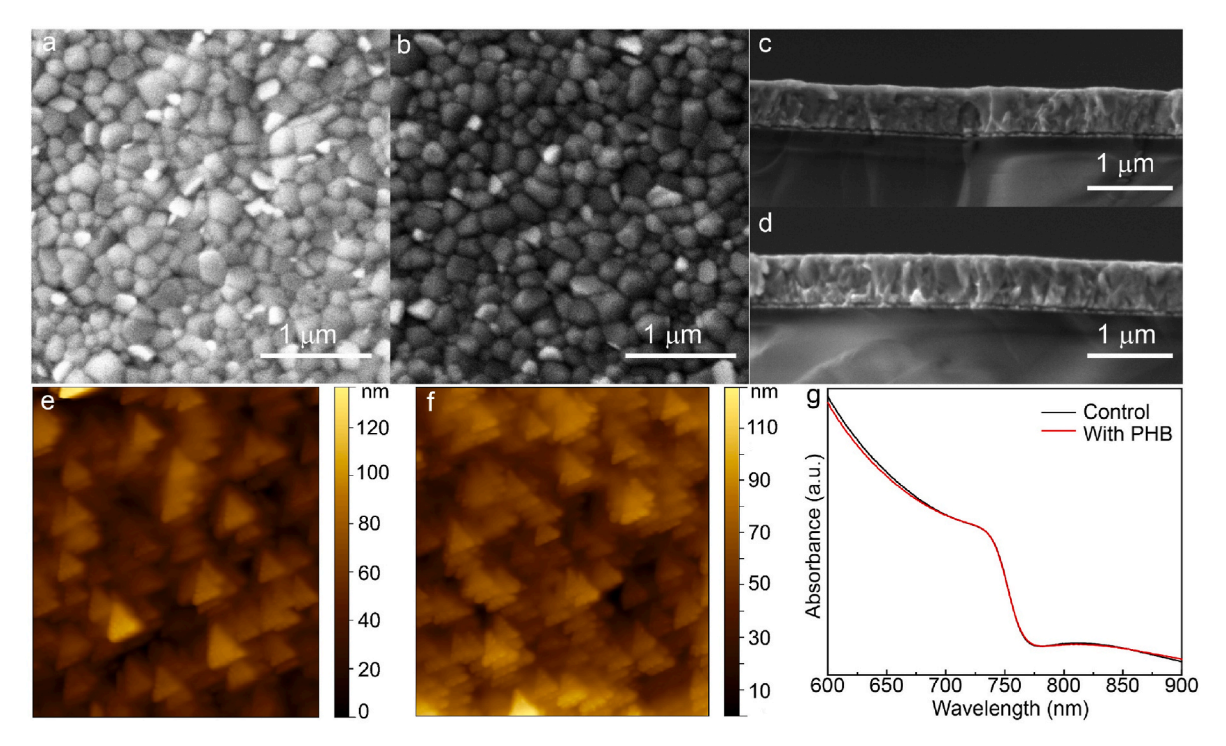


Fig. 2. a-b The top-view SEM images of perovskite films without and with PHB; c-d The cross-section SEM images of perovskite films without and with PHB; e-f The AFM images of perovskite films without and with PHB; g The UV-vis spectra of perovskite films without PHB.

dispersed in IPA by stirring in this work. After annealing, PHB has interaction with perovskite which can be seen in FTIR results. Spiro-OMeTAD solution was prepared by 72.3 mg Spiro-OMeTAD in 1 mL chlorobenzene with adding 28.8 μ L 4-tertbutylpyridine and 17.5 μ L bis (trifluoromethylsulfonyl) imide lithium solution (520 mg in 1 mL acetonitrile). 30 μ L Spiro-OMeTAD solution was spin-coated on the perovskite films as a hole-transport layer. Then, the substrates were kept in a desiccator for 12 h for oxidation. Finally, 60 nm of the gold (Au) electrode was evaporated on the top of the Spiro-MeOTAD layer under a high vacuum. The active area of devices is 0.1 cm² decided by the shadow masks.

2.3. Characterization

The perovskite film morphology and surface were studied by a field emission scanning electron microscope (LYR3 XMH, Tescan) and atomic force microscopy (AFM) (Bruker Dimension Icon Scanning Probe Microscope). The UV-vis absorption spectra were collected by Cary 60 UV-vis spectrophotometer (Agilent Technologies). The current-voltage (J-V) curves and light stability were characterised by a digital source meter (Keithley, 2400, USA) between 1.2 and 0 V at a scan rate of 10 mV/s under the illumination of the G2V Pico solar simulator AM1.5G (100 mW/cm²). The J-V and light stability measurements were performed at the temperature of 25 $^{\circ}$ C. The incident light intensity of the solar simulator was calibrated with an NREL-calibrated Si solar cell (91150 V, Newport). We also used AM 1.5G simulated sunlight (100 mW cm⁻²) (Newport) as the light source to double-check the J-V, and we got the same results. The steady-state photoluminescence (PL) spectra and the time-resolved photoluminescence (TRPL) were measured by the fluorescence spectrometer (FluoroMax, Horiba) with DeltaHub and NanoLED under 461 nm excitation. The electrochemical impedance spectroscopy (EIS) data were collected by the electrochemical workstation (CHI 604E) to study the series and recombination resistance of PSCs. The EIS measurement was swept from 1 Hz to 1 M Hz frequency with 0.9 bias voltage in the dark. The quantum efficiency measurement system (IQE-200B, Newport) was used to study the monochromatic external quantum efficiency (EQE). For the hole-only transport devices,

the J-V curves were recorded by source meter (Keithley, 2450, USA). X-ray diffraction (XRD) patterns were collected with a Rigaku Smart Lab X-ray Diffractometer.

3. Results and discussions

Fig. 1a shows the PSC structure of FTO/TiO₂/perovskite with PHB/ Spiro-OMeTAD/Au. PHB is used as a passivant on the perovskite film, and its chemical molecule structure is exhibited in the inset of Fig. 1a. Under light illumination, the electron and hole pairs are generated in the perovskite layer. The electrons are collected by the TiO2 electron transport layer, and holes are collected by the Spiro-OMeTAD layer. The FTIR spectra of the perovskite films with and without PHB are illustrated in Fig. 1b, in which the vibration of CH₃ bond shifts from 3265 cm⁻¹ to 3261 cm^{-1} as PHB is used to modify the perovskite films [28,29]. The vibration of CH3 bond shifts to a lower wavenumber after PHB passivation, indicating the interaction between PHB and perovskite [28–31]. It is usually accepted that the perovskite peaks shift to the low wavenumber side, which indicates the interaction between the passivation materials and the films. Many studies have shown similar results [29–31]. Fig. 1c displays the schematic of perovskite film passivation by PHB. The PHB has strong interaction with the uncoordinated Pb²⁺ in the perovskite due to the carbon-oxygen double bond in the structure of PHB [32]. Fig. 1d shows the XRD diffraction patterns of perovskite films with and without PHB passivation, and the peak at 12.6° is assigned to the crystal plane of (001) of PbI2. It is reported that the residual PbI2 does not affect the device performance [33]. The diffraction peaks at 14.1°, 20.0°, 24.5°, 28.3°, 31.8° and 34.9° are attributed to 100, 110, 111, 200, 210 and 211 crystal planes of perovskite films [34-37]. The PHB passivation does not influence the perovskite diffraction peaks, indicating PHB passivation doesn't affect the crystallinity of perovskite films

To investigate the effect of PHB passivation on perovskite film morphology and surface, the SEM and AFM measurements of the films with and without PHB are carried out. Fig. 2a and b shows the top-view SEM images of perovskite films without and with PHB passivation. It is clear to see that the perovskite grains densely stack together to form

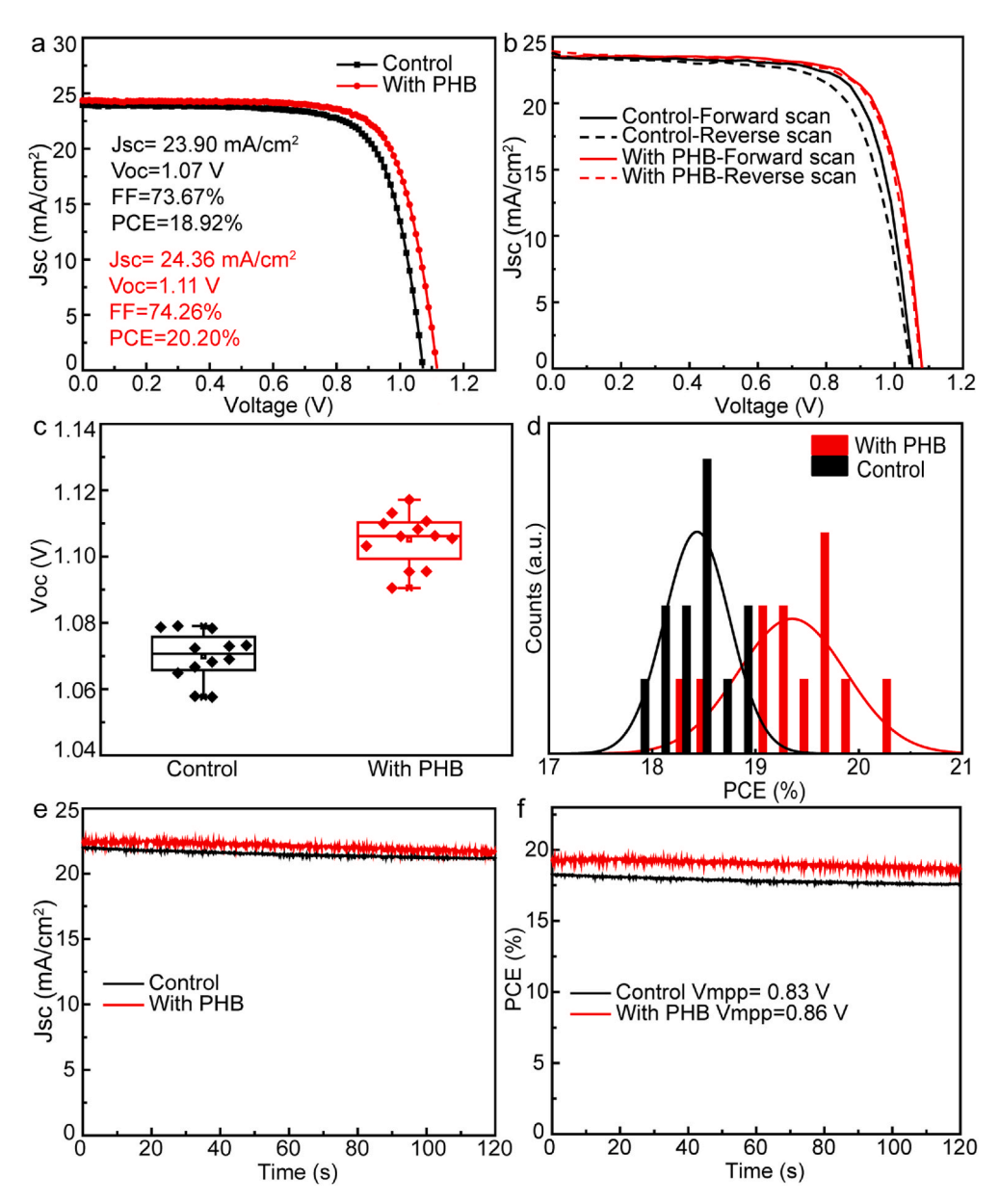


Fig. 3. a The J-V curves of PSCs with and without PHB; b The J-V curves of the PSC without and with PHB under different scan directions; c The histograms of Voc values of PSCs with and without PHB; d The PCE histograms of PCE values of PSCs with and without PHB; e-f The steady-state current density and PCE output of the PSCs with and without PHB.

films, and the average grain sizes of perovskite film with and without PHB passivation are \sim 250 nm. This result indicates the PHB passivation does not influence perovskite grains due to the post-treatment. The passivation materials are very limited on the films, but FTIR results show the existence of the PHB on the films. SEM results indicate the PHB passivation does not influence perovskite grains due to the posttreatment, which means that the passivation occurs after film growth. It is very possible that the PHB molecules are too small to be observed by SEM. Fig. 2c and d exhibit the cross-section SEM images of the perovskite layer without and with PHB. The thickness of the perovskite films with and without PHB modified are almost the same (~580 nm). The flatness of perovskite films without and with PHB passivation is measured by AFM, as illustrated in Fig. 2e and f. The root mean square (RMS) values of the perovskite films without and with PHB passivation are 66 nm and 41 nm, respectively. Thus, the PHB passivation makes the perovskite films smoother and flatter than the control perovskite films, which can improve the charge extraction and transport in the devices. The UV-vis absorption spectra in Fig. 2g shows that the control

perovskite film exhibits a little higher absorption intensity in the range of 600-700 nm than that of the one with PHB, but the authors have not explained it. The higher absorption intensity is very minor, and some published results also show very similar behavior [38-40]. Zhang et al. simply explained this by the negative effect of passivation [39]. There are two competing mechanisms involved in the light absorption process. The passivation effect increases the UV-vis absorption of the films due to the decreased defects. The other mechanism is the negative effect such as light blocking and scattering, which cause the decreased absorption. The above two mechanisms lead to the changed absorption intensity. However, it is noted that the change is very minor, which indicates the minor negative effect of the passivation. In addition, two films exhibit the same peak position at ~735 nm which is attributed to the perovskite bandgap absorption (Fig. 2g). Besides, the two peaks almost overlap, indicating the PHB passivation does not influence the light-harvesting of perovskite layers.

The PHB passivation effects on the PSC performance are studied via concentration-dependent cell measurements (Fig. S1). The average

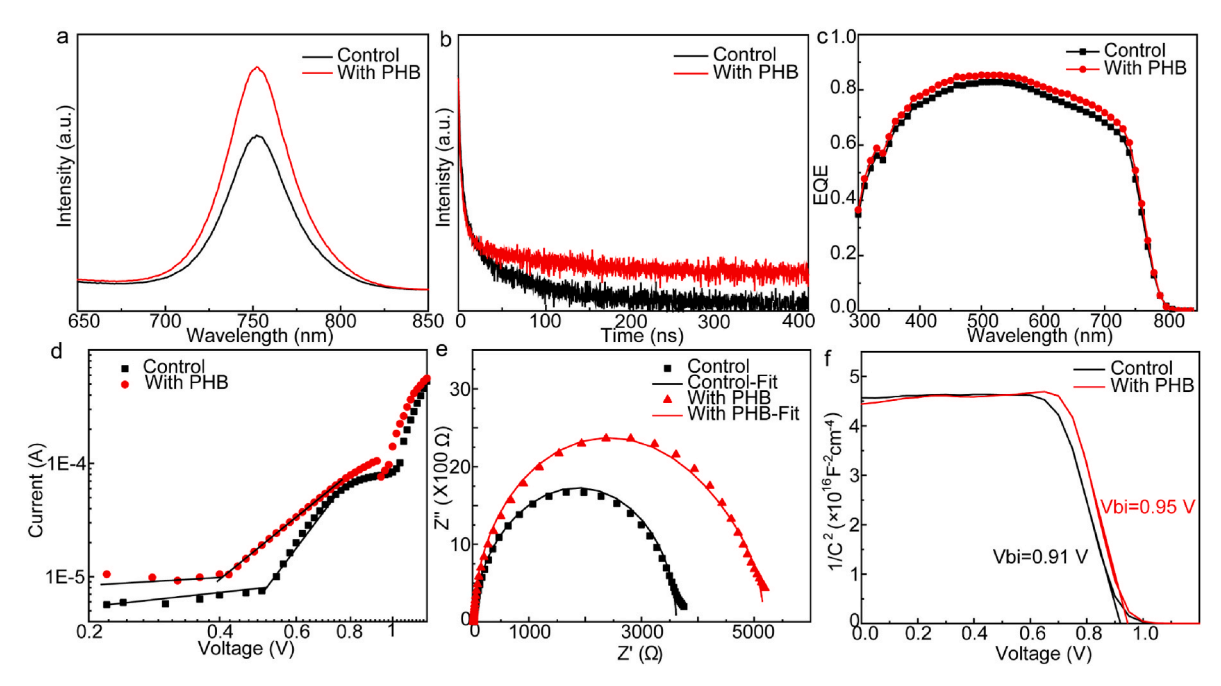


Fig. 4. a-b The PL and TRPL of perovskite films with and without PHB; c The EQE spectra of PSCs with and without PHB; d The hole-only devices with and without PHB; e Nyquist plots of PSCs with and without PHB measured in the frequency range from 1 MHz to 1 Hz at 0 V bias under dark; f Mott-Schottky measurement for PSCs with and without PHB.

device efficiency is enhanced from 17.9% to 18.7% with increasing PHB concentration from 0.15 mg/mL to 0.5 mg/mL. However, when the PHB concentration reaches to 1 mg/mL, the average PCE of PSCs decreases from 18.7% to 16.5%, so the optical concentration of PHB is 0.5 mg/mL. Fig. 3a shows the J-V curves of the optimized PSCs with and without PHB. The optimized device with PHB passivation exhibits a PCE of 20.20% with Jsc of 24.36 mA/cm², Voc of 1.11 V, and FF of 74.26%, which exhibits better performance than the control device (PCE = 18.92%, Jsc = 23.90 mA/cm², Voc = 1.07 V and FF = 73.67%). Therefore, PHB passivation enhances the performance of devices, which is attributed to the decreased defects and traps in the films due to PHB passivation. Fig. 3b illustrates the performance of PSCs with and without PHB under different scan directions. The hysteresis index values can be calculated by the following equation:

$$HI = \frac{PCE_{reverse} - PCE_{forward}}{PCE_{reverse}}$$

where PCE_{reverse} is the PCE of the devices with reverse scan direction, and PCEforward is the PCE obtained under forward scan direction. The PCE values of control devices with reverse and forward scan directions are 18.53% and 17.40%, respectively, and the HI value is calculated to be 0.061. For the PSCs with PHB, the PCE values are 19.28% and 19.24%for the reverse and forward scan directions, respectively, and the HI value is 0.002, which is a very small HI value for normal PSCs. Therefore, PHB passivation decreases the hysteretic effect of the PSCs significantly, indicating that PHB passivation suppresses the charge recombination and inhibits the ion migration at the interface [41-43]. PHB passivation enhances the Voc and further improves the PCE of the PSCs, as illustrated in Fig. 3c and d. The control PSCs exhibit the average PCE of \sim 18.5% with the average Voc is \sim 1.07 V, and the average PCE of devices with PHB passivation is 19.8% with the average Voc is \sim 1.15 V. Voc is significantly increased, leading to enhanced PCE, which is attributed to the decreased defects and traps at the interface of perovskite and hole-transport layer due to PHB passivation effect [44,45]. The photocurrent density and PCE stability plots of devices with and without PHB passivation under continuous light irradiation for 125 s are shown in Fig. 3e and f. The control PSC shows a current density of 21.18 mA/cm² and the PCE of 17.60% with the maximum output power

voltage (Vmpp) of 0.83 V. However, the device with PHB exhibits the current density of $21.68~\text{mA/cm}^2$ and the PCE of 18.65% under the Vmpp of 0.86~V.

To study the influence of PHB passivation on the charge recombination process of the PSCs, the steady-state photoluminescence (PL) is measured, as illustrated in Fig. 4a. The PL spectra of the perovskite film after treatment by PHB exhibits higher intensity than the control perovskite film, which indicates decreased non-radiative recombination in films by PHB passivation [46]. Fig. 4b exhibits the time-resolved photoluminescence (TRPL) plots of the films with and without PHB, and the data are fitted by the following biexponential decay function.

$$Y = A_1 \exp(\frac{-t}{\tau_1}) + A_2 \exp(\frac{-t}{\tau_2})$$

where $\tau 1$ and $\tau 2$ are the values of the lifetime for the fast and slow decay, respectively. A1 and A2 are the relative amplitudes. The fast decay $(\tau 1)$ is assigned to charge trapping in the defects in the perovskite films, and the slow decay $(\tau 2)$ is attributed to the radiative recombination [42,47]. The fitted $\tau 1$ and $\tau 2$ of control perovskite film are 47.8 ns and 191.3 ns, respectively. Besides, the fitted lifetime $\tau 1$ and $\tau 2$ for the perovskite film with PHB passivation are 85.6 ns and 342.7 ns, respectively. After the PHB treatment, $\tau 2$ increases from 191.3 ns to 342.7 ns. PHB passivation suppresses the charge recombination and further enhances the carrier lifetime in perovskite films. Fig. 4c shows the EQE curves of the PSCs with and without PHB passivation. The photoresponse of PSCs with and without PHB passivation range from 300 nm to 850 nm, but the PSC with PHB shows a little higher photoresponse. PHB passivation increases the carrier extraction and transfer in the devices, which further improves the PCE of the PSCs [48,49]. The integrated Jsc of the optimized modified device is 19.9 mA/cm² compared to 24.36 mA/cm² obtained from the J-V measurements (Fig. S2). Recently, Etgar et al. reported that the integrated current density from IPCE is reasonable to be less than the Jsc from J-V measurement within 10-20% [50]. The inconsistency is attributed to the light sources, ion migration, and degradation during IPCE measurement caused by long-time light irradiation, ion movement due to the bias, and frequency-dependent IPCE measurements. The hole-only devices with structure of FTO/PTAA/perovskite/Spiro-OMeTAD/Au are

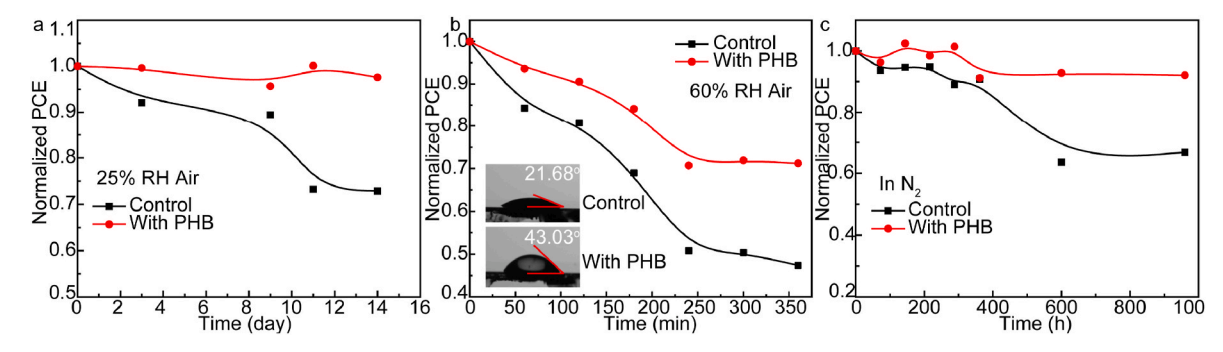


Fig. 5. a The stability of PSCs with and without PHBs in an ambient environment with RH condition of $25 \pm 5\%$; b The stability of PSCs and water contact angle of perovskite films with and without PHB in an environment with an RH condition of $60 \pm 5\%$; c The stability of PSCs with and without PHB in N_2 environment.

fabricated to evaluate the hole defect density in the PSCs with and without PHB passivation, as illustrated in Fig. 4d. Three behaviors in J-V curves of the hole-only devices include an ohmic region (n=1), a trap-filled limit (TFL) region (n>3), and a space-charge limited current (SCLC) region (n=2) [51,52]. Besides, the hole trap density can be calculated by the following equation:

$$V_{TFL} = \frac{en_t L^2}{2\varepsilon\varepsilon_0}$$

where n_t is the defect density in the perovskite film; V_{TFL} is the onset voltage in the TFL region; e is the elementary charge of an electron; L is the perovskite film thickness; ε is the relative dielectric constant of MAPbI₃ and ε_0 is the vacuum dielectric constant. The calculated hole defect density values for the control device and the device with PHB passivation are $1.26 \times 10^{18} \text{ cm}^{-3}$ and $9.89 \times 10^{17} \text{ cm}^{-3}$, respectively. The reduced hole trap density is attributed by PHB passivation. The Nyquist plots are shown in Fig. 4e, and the equivalent circuit used for fitting is illustrated in the inset of Fig. 4e. The series resistance(Rs) decreases from 32.48 Ω to 21.24 Ω , and the charge recombination resistance Rrec increases from 2044 Ω to 4424 Ω after PHB passivation treatment. These results indicate PHB passivation improves the charge transport and suppresses the exciton recombination at the interface of the perovskite layer/Spiro-OMeTAD layer [53,54], which also explains the increased Voc. In addition, the heterojunction properties of the interface between the perovskite layer and Spiro-OMeTAD layer are studied by capacitance-voltage (C-V) measurements. The 1/C2 plots of PSCs with and without PHB passivation are illustrated in Fig. 4f. The V_{bi} values of the PSCs with and without PHB passivation are 0.95 V and 0.91 V, respectively. This result indicates PHB passivation improves the carrier diffusion and carrier injection in the interface [55], which further explain the increased Voc caused by PHB passivation (1.07 V-1.11 V) (Fig. 3c).

Furthermore, we also investigate the moisture and long-term stability of the PSCs with and without PHB passivation. Fig. 5a shows the long-term stability of the PSCs under 25 \pm 5% relative humidity (RH) and 30 \pm 5 $^{\circ}$ C conditions for 14 days. The device without PHB passivation degrades to ~72% of the initial PCE, whereas the PCE of the device with PHB treatment still exhibits ~98% of its initial PCE. In addition, the moisture stability of the PSCs with and without PHB passivation is measured under 60 \pm 5% RH and 30 \pm 5 °C conditions, as displayed in Fig. 5b. The device with PHB can keep ~75% of the original values of PCE, but the control device only can maintain \sim 45% of the initial values for 350 min. The water contact angle images with perovskite films with and without PHB are shown in the inset of Fig. 5b. The water contact angle values of the perovskite films with and without PHB are 43.03° and 21.68°, respectively. The stability of PSCs with and without PHB passivation is shown in Fig. 5c, which suggests the devices with PHB passivation could keep 92% of the initial PCE value but control device only maintains 66% of the initial PCE. These results demonstrate the PHB passivation improves the stability of devices. The improved device

stability is attributed to the hydrophobic properties of the alkyl chains on PHB.

4. Conclusions

In summary, we study a multifunctional passivation strategy, in which the C=O functional groups in the PHB structure are in situ modify the defects and traps in the perovskite film by the interaction with Pb $^{2+}$. The PHB passivation suppresses the nonradiative recombination and decreases the hole traps in the PSCs, which are confirmed with the PL, TRPL, EIS measurements. The PCE of PSCs increases from 18.92% to 20.20%, and the average Voc increases from 1.07 V to 1.11 V after PHB passivation. The PHB passivation can protect the devices from degradation due to the hydrophobicity of PHB caused by alkyl chains. As the devices are exposed in $60\pm5\%$ RH for 350 min (30 \pm 5 °C), the device with PHB keeps $\sim\!\!75\%$ of the original value of PCE, but the control device only can maintain $\sim\!\!45\%$ of the initial value. Besides, the device without PHB passivation degrades to $\sim\!\!72\%$ of the initial PCE, whereas the PCE of the device with PHB exhibits only a little decrease as the devices are kept under $25\pm5\%$ RH and 30 ± 5 °C condition for 14 days.

Declaration of competing interest

The authors declare that they have no known competing financial interests or personal relationships that could have appeared to influence the work reported in this paper.

Acknowledgment

This material is based on work supported by the National Science Foundation under Grant No. 1757220. The steady-state PL and TRPL equipment used in this work is supported by National Science Foundation Research Initiation Award: Novel Perovskite Solar Cells Based on Interface Manipulation (Award#1900047).

Appendix A. Supplementary data

Supplementary data to this article can be found online at https://doi.org/10.1016/j.orgel.2022.106487.

References

- [1] M. Yang, Z. Li, M.O. Reese, O.G. Reid, D.H. Kim, S. Siol, T.R. Klein, Y. Yan, J. J. Berry, M.F.A.M. van Hest, K. Zhu, Perovskite ink with wide processing window for scalable high-efficiency solar cells, Nat. Energy 2 (2017), https://doi.org/10.1038/nenergy.2017.38.
- [2] X. Li, M. Ibrahim Dar, C. Yi, J. Luo, M. Tschumi, S.M. Zakeeruddin, M. K. Nazeeruddin, H. Han, M. Grätzel, Improved performance and stability of perovskite solar cells by crystal crosslinking with alkylphosphonic acid ω-ammonium chlorides, Nat. Chem. 7 (2015) 703–711, https://doi.org/10.1038/nchem.2324.
- [3] Z. Huanping, C. Qi, L. Gang, L. Song, S. Tze-bing, D. Hsin-Sheng, H. Ziruo, Y. Jingbi, L. Yongsheng, Y. Yang, Interface engineering of highly efficient

- perovskite solar cells, 80-, Science 345 (2014) 542–546, https://doi.org/10.1126/science 1254050
- [4] D. Di Girolamo, N. Phung, F.U. Kosasih, F. Di Giacomo, F. Matteocci, J.A. Smith, M. A. Flatken, H. Köbler, S.H. Turren Cruz, A. Mattoni, L. Cinà, B. Rech, A. Latini, G. Divitini, C. Ducati, A. Di Carlo, D. Dini, A. Abate, Ion migration-induced amorphization and phase segregation as a degradation mechanism in planar perovskite solar cells, Adv. Energy Mater. 10 (2020), 2000310, https://doi.org/10.1002/aenm.202000310.
- [5] D. Zhao, C. Chen, C. Wang, M.M. Junda, Z. Song, C.R. Grice, Y. Yu, C. Li, B. Subedi, N.J. Podraza, X. Zhao, G. Fang, R.-G. Xiong, K. Zhu, Y. Yan, Efficient two-terminal all-perovskite tandem solar cells enabled by high-quality low-bandgap absorber layers, Nat. Energy 3 (2018) 1093–1100, https://doi.org/10.1038/s41560-018-0278.x
- [6] L. Meng, J. You, Y. Yang, Addressing the stability issue of perovskite solar cells for commercial applications, Nat. Commun. 9 (2018), https://doi.org/10.1038/ s41467-018-07255-1.
- [7] Y. Yang, M. Yang, Z. Li, R. Crisp, K. Zhu, M.C. Beard, Comparison of recombination dynamics in CH3NH3PbBr3 and CH3NH3PbI3 perovskite films: influence of exciton binding energy, J. Phys. Chem. Lett. 6 (2015) 4688–4692, https://doi.org/ 10.1021/ces/inclust/5502300.
- [8] K. Galkowski, A. Mitioglu, A. Miyata, P. Plochocka, O. Portugall, G.E. Eperon, J.T.-W. Wang, T. Stergiopoulos, S.D. Stranks, H.J. Snaith, R.J. Nicholas, Determination of the exciton binding energy and effective masses for methylammonium and formamidinium lead tri-halide perovskite semiconductors, Energy Environ. Sci. 9 (2016) 962–970, https://doi.org/10.1039/c5ee03435c.
- [9] K. Minjin, J. Jaeki, L. Haizhou, L.T. Kyung, E.F. T, L. Yuhang, C.I. Woo, C.S. Ju, J. Yimhyun, K. Hak-Beom, M. Sung-In, K. Young-Ki, L. Heunjeong, A.N. Gyeong, C. Shinuk, T.W. R, Z.S. M, H. Anders, K.J. Young, G. Michael, K.D. Suk, Conformal quantum dot–SnO2 layers as electron transporters for efficient perovskite solar cells, 80-, Science 375 (2022) 302–306, https://doi.org/10.1126/science.abh1885.
- [10] C.C. Boyd, R. Cheacharoen, T. Leijtens, M.D. McGehee, Understanding degradation mechanisms and improving stability of perovskite photovoltaics, Chem. Rev. 119 (2018) 3418–3451, https://doi.org/10.1021/acs.chemrev.8b00336.
- [11] Y. Shao, Y. Fang, T. Li, Q. Wang, Q. Dong, Y. Deng, Y. Yuan, H. Wei, M. Wang, A. Gruverman, J. Shield, J. Huang, Grain boundary dominated ion migration in polycrystalline organic–inorganic halide perovskite films, Energy Environ. Sci. 9 (2016) 1752–1759, https://doi.org/10.1039/c6ee00413j.
- [12] R. Garai, R.K. Gupta, A.S. Tanwar, M. Hossain, P.K. Iyer, Conjugated polyelectrolyte-passivated stable perovskite solar cells for efficiency beyond 20, Chem. Mater 33 (2021) 5709–5717, https://doi.org/10.1021/acs. chemmater.101436.
- [13] J. Ávila, C. Momblona, P.P. Boix, M. Sessolo, H.J. Bolink, Vapor-deposited perovskites: the route to high-performance solar cell production? Joule 1 (2017) 431–442, https://doi.org/10.1016/j.joule.2017.07.014.
- [14] M. Liu, M.B. Johnston, H.J. Snaith, Efficient planar heterojunction perovskite solar cells by vapour deposition, Nature 501 (2013) 395–398, https://doi.org/10.1038/ nature12509.
- [15] M.T. Hoerantner, E.L. Wassweiler, H. Zhang, A. Panda, M. Nasilowski, A. Osherov, R. Swartwout, A.E. Driscoll, N.S. Moody, M.G. Bawendi, K.F. Jensen, V. Bulović, High-speed vapor transport deposition of perovskite thin films, ACS Appl. Mater. Interfaces 11 (2019) 32928–32936, https://doi.org/10.1021/acsami.9b07651.
- [16] Y. Chen, Q. Meng, Y. Xiao, X. Zhang, J. Sun, C.B. Han, H. Gao, Y. Zhang, Y. Lu, H. Yan, Mechanism of PbI2 in situ passivated perovskite films for enhancing the performance of perovskite solar cells, ACS Appl. Mater. Interfaces 11 (2019) 44101–44108, https://doi.org/10.1021/acsami.9b13648.
- [17] A. Mahapatra, D. Prochowicz, M.M. Tavakoli, S. Trivedi, P. Kumar, P. Yadav, A review of aspects of additive engineering in perovskite solar cells, J. Mater. Chem. A. 8 (2020) 27–54, https://doi.org/10.1039/c9ta07657c.
- [18] R. Garai, M.A. Afroz, R.K. Gupta, P.K. Iyer, Efficient trap passivation of MAPbI 3 via multifunctional anchoring for high-performance and stable perovskite solar cells, Adv. Sustain. Syst. 4 (2020), 2000078, https://doi.org/10.1002/ adsu.202000078.
- [19] M. Adil Afroz, N. Ghimire, K.M. Reza, B. Bahrami, R.S. Bobba, A. Gurung, A. H. Chowdhury, P.K. Iyer, Q. Qiao, Thermal stability and performance enhancement of perovskite solar cells through oxalic acid-induced perovskite formation, ACS Appl. Energy Mater. 3 (2020) 2432–2439, https://doi.org/10.1021/acsaem_9h02111
- [20] T.-H. Han, J.-W. Lee, C. Choi, S. Tan, C. Lee, Y. Zhao, Z. Dai, N. De Marco, S.-J. Lee, S.-H. Bae, Y. Yuan, H.M. Lee, Y. Huang, Y. Yang, Perovskite-polymer composite cross-linker approach for highly-stable and efficient perovskite solar cells, Nat. Commun. 10 (2019), https://doi.org/10.1038/s41467-019-08455-z.
- [21] M. Zhong, L. Chai, Y. Wang, J. Di, Enhanced efficiency and stability of perovskite solar cell by adding polymer mixture in perovskite photoactive layer, J. Alloys Compd. 864 (2021), 158793, https://doi.org/10.1016/j.jallcom.2021.158793.
- [22] D. Bi, C. Yi, J. Luo, J.-D. Décoppet, F. Zhang, S.M. Zakeeruddin, X. Li, A. Hagfeldt, M. Grätzel, Polymer-templated nucleation and crystal growth of perovskite films for solar cells with efficiency greater than 21, Nat. Energy 1 (2016), https://doi. org/10.1038/nenergy.2016.142.
- [23] F. Li, J. Yuan, X. Ling, Y. Zhang, Y. Yang, S.H. Cheung, C.H.Y. Ho, X. Gao, W. Ma, A universal strategy to utilize polymeric semiconductors for perovskite solar cells with enhanced efficiency and longevity, Adv. Funct. Mater. 28 (2018), 1706377, https://doi.org/10.1002/adfm.201706377.
- [24] Y.-C. Wang, J. Chang, L. Zhu, X. Li, C. Song, J. Fang, Electron-transport-layer-assisted crystallization of perovskite films for high-efficiency planar heterojunction solar cells, Adv. Funct. Mater. 28 (2017), 1706317, https://doi.org/10.1002/adfm.201706317.

- [25] J. Yang, W. Tang, R. Yuan, Y. Chen, J. Wang, Y. Wu, W.-J. Yin, N. Yuan, J. Ding, W.-H. Zhang, Defect mitigation using d-penicillamine for efficient methylammonium-free perovskite solar cells with high operational stability, Chem. Sci. 12 (2021) 2050–2059, https://doi.org/10.1039/d0sc06354a.
- [26] X. Yu, Y. Lv, B. Xue, L. Wang, W. Hu, X. Liu, S. Yang, W.-H. Zhang, Multiple bonding effects of 1-methanesulfonyl-piperazine on the two-step processed perovskite towards efficient and stable solar cells, Nano Energy 93 (2022), 106856, https://doi.org/10.1016/j.nanoen.2021.106856.
- [27] W. Rui, X. Jingjing, W. Kai-Li, W. Zhao-Kui, L. Yanqi, F. David, X. Guangwei, N. Selbi, H. Tianyi, Z. Yepin, Y.J. Lee, Z. Jiahui, W. Minhuan, T. Shaun, Y. Ilhan, H. K. N, Y. Yang, Constructive molecular configurations for surface-defect passivation of perovskite photovoltaics, Science 366 (2019) 1509–1513, https://doi.org/10.1126/science.aay9698, 80-.
- [28] S. Akin, E. Akman, S. Sonmezoglu, FAPbI 3 -based perovskite solar cells employing hexyl-based ionic liquid with an efficiency over 20% and excellent long-term stability, Adv. Funct. Mater. 30 (2020), 2002964, https://doi.org/10.1002/ adfm.202002964.
- [29] T. Glaser, C. Müller, M. Sendner, C. Krekeler, O.E. Semonin, T.D. Hull, O. Yaffe, J. S. Owen, W. Kowalsky, A. Pucci, R. Lovrinčić, Infrared spectroscopic study of vibrational modes in methylammonium lead halide perovskites, J. Phys. Chem. Lett. 6 (2015) 2913–2918, https://doi.org/10.1021/acs.jpclett.5b01309.
- [30] S.-H. Lee, S. Jeong, S. Seo, H. Shin, C. Ma, N.-G. Park, Acid dissociation constant: a criterion for selecting passivation agents in perovskite solar cells, ACS Energy Lett (2021) 1612–1621, https://doi.org/10.1021/acsenergylett.1c00452.
- [31] W. Zhao, J. Xu, K. He, Y. Cai, Y. Han, S. Yang, S. Zhan, D. Wang, Z. Liu, S. Liu, A special additive enables all cations and anions passivation for stable perovskite solar cells with efficiency over 23, Nano-Micro Lett. 13 (2021), https://doi.org/10.1007/s40820-021-00688-2.
- [32] J. Peng, J.I. Khan, W. Liu, E. Ugur, T. Duong, Y. Wu, H. Shen, K. Wang, H. Dang, E. Aydin, X. Yang, Y. Wan, K.J. Weber, K.R. Catchpole, F. Laquai, S. Wolf, T. P. White, A universal double-side passivation for high open-circuit voltage in perovskite solar cells: role of carbonyl groups in poly(methyl methacrylate), Adv. Energy Mater. 8 (2018), 1801208, https://doi.org/10.1002/aenm.201801208.
- [33] Y.H. Lee, J. Luo, R. Humphry-Baker, P. Gao, M. Grätzel, M.K. Nazeeruddin, Unraveling the reasons for efficiency loss in perovskite solar cells, Adv. Funct. Mater. 25 (2015) 3925–3933, https://doi.org/10.1002/adfm.201501024.
- [34] E.T. Hoke, D.J. Slotcavage, E.R. Dohner, A.R. Bowring, H.I. Karunadasa, M. D. McGehee, Reversible photo-induced trap formation in mixed-halide hybrid perovskites for photovoltaics, Chem. Sci. 6 (2015) 613–617, https://doi.org/10.1039/c4sc03141e
- [35] M. Saliba, T. Matsui, J.-Y. Seo, K. Domanski, J.-P. Correa-Baena, M.K. Nazeeruddin, S.M. Zakeeruddin, W. Tress, A. Abate, A. Hagfeldt, M. Grätzel, Cesium-containing triple cation perovskite solar cells: improved stability, reproducibility and high efficiency, Energy Environ. Sci. 9 (2016) 1989–1997, https://doi.org/10.1039/c5ee03874i.
- [36] Y. Hu, M.F. Aygüler, M.L. Petrus, T. Bein, P. Docampo, Impact of rubidium and cesium cations on the moisture stability of multiple-cation mixed-halide perovskites, ACS Energy Lett 2 (2017) 2212–2218, https://doi.org/10.1021/ acsenergylett.7b00731.
- [37] L. Zhu, X. Zhang, M. Li, X. Shang, K. Lei, B. Zhang, C. Chen, S. Zheng, H. Song, J. Chen, Trap state passivation by rational ligand molecule engineering toward efficient and stable perovskite solar cells exceeding 23% efficiency, Adv. Energy Mater. 11 (2021), 2100529. https://doi.org/10.1109/aepm.2021.00529
- Mater. 11 (2021), 2100529, https://doi.org/10.1002/aenm.202100529.

 [38] H. Zhang, Y. Wu, C. Shen, E. Li, C. Yan, W. Zhang, H. Tian, L. Han, W. Zhu, Efficient and stable chemical passivation on perovskite surface via bidentate anchoring, Adv. Energy Mater. 9 (2019), 1803573, https://doi.org/10.1002/
- [39] D. Xin, S. Tie, R. Yuan, X. Zheng, J. Zhu, W.-H. Zhang, Defect passivation in hybrid perovskite solar cells by tailoring the electron density distribution in passivation molecules, ACS Appl. Mater. Interfaces 11 (2019) 44233–44240, https://doi.org/ 10.1021/acsami.9b15166.
- [40] W. Sun, J. Zou, X. Wang, S. Wang, Y. Du, F. Cao, L. Zhang, J. Wu, P. Gao, Enhanced photovoltage and stability of perovskite photovoltaics enabled by a cyclohexylmethylammonium iodide-based 2D perovskite passivation layer, Nanoscale 13 (2021) 14915–14924, https://doi.org/10.1039/d1nr03624f.
- [41] C. Geffroy, E. Grana, T. Bessho, S. Almosni, Z. Tang, A. Sharma, T. Kinoshita, F. Awai, E. Cloutet, T. Toupance, H. Segawa, G. Hadziioannou, p-Doping of a hole transport material via a poly(ionic liquid) for over 20% efficiency and hysteresisfree perovskite solar cells, ACS Appl. Energy Mater. 3 (2020) 1393–1401, https://doi.org/10.1021/acsaem.9b01819.
- [42] D.-H. Kang, N.-G. Park, On the current-voltage hysteresis in perovskite solar cells: dependence on perovskite composition and methods to remove hysteresis, Adv. Mater. 31 (2019), 1805214, https://doi.org/10.1002/adma.201805214.
- [43] J. Chen, N.-G. Park, Materials and methods for interface engineering toward stable and efficient perovskite solar cells, ACS Energy Lett 5 (2020) 2742–2786, https:// doi.org/10.1021/acsenergylett.0c01240.
- [44] Q. Zhou, Q. Xiong, Z. Zhang, J. Hu, F. Lin, L. Liang, T. Wu, X. Wang, J. Wu, B. Zhang, P. Gao, Fluoroaromatic cation-assisted planar junction perovskite solar cells with improved V OC and stability: the role of fluorination position, Sol. RRL 4 (2020), 2000107, https://doi.org/10.1002/solr.202000107.
- [45] S. Kim, J.H. Jang, Z. Wu, M.J. Lee, H.Y. Woo, I. Hwang, Interfacial defects change the correlation between photoluminescence, ideality factor, and open-circuit voltage in perovskite solar cells, Small 17 (2021), 2101839, https://doi.org/ 10.1002/smll.202101839.

- [46] C. Ma, N.-G. Park, Paradoxical approach with a hydrophilic passivation layer for moisture-stable, 23% efficient perovskite solar cells, ACS Energy Lett 5 (2020) 3268–3275, https://doi.org/10.1021/acsenergylett.0c01848.
- [47] B. Liu, H. Bi, D. He, L. Bai, W. Wang, H. Yuan, Q. Song, P. Su, Z. Zang, T. Zhou, J. Chen, Interfacial defect passivation and stress release via multi-active-site ligand anchoring enables efficient and stable methylammonium-free perovskite solar cells, ACS Energy Lett 6 (2021) 2526–2538, https://doi.org/10.1021/acsenergylett.1c00794.
- [48] M. Hou, Y. Xu, B. Zhou, Y. Tian, Y. Wu, D. Zhang, G. Wang, B. Li, H. Ren, Y. Li, Q. Huang, Y. Ding, Y. Zhao, X. Zhang, G. Hou, Aryl diammonium iodide passivation for efficient and stable hybrid organ-inorganic perovskite solar cells, Adv. Funct. Mater. 30 (2020), 2002366, https://doi.org/10.1002/adfm.202002366
- [49] Z. Liu, F. Cao, M. Wang, M. Wang, L. Li, Observing defect passivation of the grain boundary with 2-aminoterephthalic acid for efficient and stable perovskite solar cells, Angew. Chem. Int. Ed. 59 (2020) 4161–4167, https://doi.org/10.1002/ anie.201915422.
- [50] M. Saliba, L. Etgar, Current density mismatch in perovskite solar cells, ACS Energy Lett 5 (2020) 2886–2888, https://doi.org/10.1021/acsenergylett.0c01642.

- [51] E.A. Duijnstee, J.M. Ball, V.M. Le Corre, L.J.A. Koster, H.J. Snaith, J. Lim, Toward understanding space-charge limited current measurements on metal halide perovskites, ACS Energy Lett 5 (2020) 376–384, https://doi.org/10.1021/ acseneroylett 9h02720
- [52] M. Sajedi Alvar, P.W.M. Blom, G.-J.A.H. Wetzelaer, Space-charge-limited electron and hole currents in hybrid organic-inorganic perovskites, Nat. Commun. 11 (2020), https://doi.org/10.1038/s41467-020-17868-0.
- [53] M.M. Tavakoli, R. Tavakoli, S. Hasanzadeh, M.H. Mirfasih, Interface engineering of perovskite solar cell using a reduced-graphene scaffold, J. Phys. Chem. C 120 (2016) 19531–19536, https://doi.org/10.1021/acs.jpcc.6b05667.
- [54] E. Guillén, F.J. Ramos, J.A. Anta, S. Ahmad, Elucidating transport-recombination mechanisms in perovskite solar cells by small-perturbation techniques, J. Phys. Chem. C 118 (2014) 22913–22922, https://doi.org/10.1021/jp5069076.
- [55] C. Liu, C. Igci, Y. Yang, O.A. Syzgantseva, M.A. Syzgantseva, K. Rakstys, H. Kanda, N. Shibayama, B. Ding, X. Zhang, V. Jankauskas, Y. Ding, S. Dai, P.J. Dyson, M. K. Nazeeruddin, Dopant-free hole transport materials afford efficient and stable inorganic perovskite solar cells and modules, Angew. Chem. Int. Ed. 60 (2021) 20489–20497, https://doi.org/10.1002/anie.202107774.